Available online at www.sciencedirect.com
ScienceDirect
Atmospheric Environment 40 (2006) 5533–5542
ATMOSPHERIC ENVIRONMENT
www.elsevier.com/locate/atmosenv

Nanostructure of atmospheric soot particles

Viktória Kovács Kis[a,*], Mihály Pósfai[b], János L. Lábár[a]

[a]Research Institute for Technical Physics and Materials Science, H-1525 Budapest, P.O. Box 49, Hungary
[b]Department of Earth and Environmental Sciences, Pannon University, H-8201 Veszprém, P.O. Box 158, Hungary

Received 17 January 2006; received in revised form 9 May 2006; accepted 10 May 2006

Abstract

We studied the structure of atmospheric soot using electron-diffraction-based pair distribution function (PDF) analysis, and compared it with other carbon structures. Two reference materials were used: hydrogen-free amorphous carbon and a kerogen sample with a H/C ratio of 0.61. First-neighbour atomic distances in atmospheric soot are as small as 0.134 nm, much shorter than in graphite (0.142 nm) or in amorphous carbon (0.141–143 nm), but larger than the typical value (0.131–0.132 nm) for kerogen. These results suggest that a high molar ratio of hydrogen is present in soot in small-sized aromatic clusters. Such aromatic components can strongly influence the optical properties of soot particles. We found that the quantitative electron diffraction method is an independent and efficient alternative to the commonly used spectroscopic methods for the analysis of the atomic structure of individual soot particles.

Keywords: Soot; Nanostructure; Electron diffraction; Aromatic structures

1. Introduction

The term 'soot' is used for carbonaceous particles that are produced by the combustion of fossil fuels or vegetation, and have characteristic morphology, size and microstructure (Gelencsér, 2004). As the strongest absorbent of shortwave radiation in the atmosphere, soot (or 'black carbon') has a strong influence on the radiation balance of the Earth (Jacobson, 2001; Penner et al., 2003).

The term 'black carbon' is frequently used to emphasise the absorption properties of carbonaceous material. Black carbon is considered to be a mixture of ''graphite-like'', elementary carbon and light-absorbing organic matter (Andreae, 2001). Thermal and optical methods are routinely used for the determination of light-absorbing properties of carbonaceous aerosol particles. The results obtained by these methods depend strongly on operational conditions, leading in many cases to a significant under- or overestimation of the amount of elemental (''graphite-like'') and organic carbon, the two main components that are quantified (Schmid et al., 2001).

In order to be able to assess the optical properties of atmospheric soot, detailed information on its structure is required. The widely accepted structural model for soot assumes the presence of graphene sheets that consist of a net of hexagons formed by carbon atoms, as in graphite (Bockhorn, 1994). The stacking of concentrically wrapped, curved graphene sheets results in a typical onion-like structure

*Corresponding author. Tel.: +36 1 3922791; fax: +36 1 3922273.
E-mail address: kis@mfa.kfki.hu (V.K. Kis).

1352-2310/$ - see front matter © 2006 Elsevier Ltd. All rights reserved.
doi:10.1016/j.atmosenv.2006.05.012

(Pósfai et al., 1999; Wentzel et al., 2003). However, it has long been known from bulk spectroscopic studies that soot formation involves the growth of layers from aromatic rings (Abrahamson, 1977; Lahaye, 1992; Apicella et al., 2004), and that soot contains other elements besides carbon. The chemical composition of soot depends strongly on its source and the combustion conditions. Up to 50% of the mass of soot can be organic matter (Gelencsér, 2004). Thermal measurements show a H/C molar ratio of 0.15 in atmospheric soot samples (Huffman, 1996). These compositional data are inconsistent with a structure that consists of mainly graphite-like, elementary carbon layers.

The optical properties of soot depend strongly on its structure. Specific radiation absorption is determined by bond lengths, bond energies and vibrational properties, providing the basis for spectroscopic methods that are used for deducing the bonding structure. For example, graphite, the sp^2 form of elemental carbon, has characteristic Raman modes which allow the quantitative measurement of the concentration of graphitic carbon in aerosol samples (Bond et al., 1999; Mertes et al., 2004). However, spectroscopy, as well as thermal methods, provide averaged information over a large volume of carbonaceous material. Direct measurements of the atomic level organisation of nanostructures in soot particles, and the identification of distinct local structures is an intriguing field both in atmospheric and in material sciences.

Transmission electron microscopy is well suited for the morphological and chemical characterisation of individual particles. The dependence of soot nanostructure on temperature and production rate was studied by Vander Wal and Tomasek (2004) using high-resolution transmission electron microscopy (HRTEM). They characterised the nanostructure by the sizes and physical relationships of fragments of the graphitic layer. Onion-like nanostructure was identified in HRTEM images of a "fullerenic" carbonaceous material that was produced in diffusion flames, and characterised by a curvature parameter (Goel et al., 2002). Since soot nanoparticles are spherical, only a cross-section of the spherules and the wrapped structure is revealed by HRTEM images. The atomic arrangements within the curved layers remain hidden. Therefore, although HRTEM and conventional selected-area electron diffraction (SAED) methods are very useful for a general characterisation of soot structure, they do not provide an insight into the local structures within the graphene-like sheets.

The bonding configuration can be deduced from electron-energy loss (EEL) spectroscopy. Katrinak et al. (1992) measured the energy difference of σ^* and π^* peaks in the EEL spectra of urban atmospheric soot and deduced that both the aggregates and the individual spherules are mixtures of graphite and hydrocarbons.

In the present study, we apply SAED in a quantitative way to the investigation of the atomic arrangement in individual soot particles from atmospheric aerosol. Even though soot is amorphous, SAED patterns provide useful information about its structure. By quantitatively measuring the radial distribution of the diffracted intensity, it is possible to obtain information on the local structure, in the form of frequency distributions of interatomic distances.

Our results are interpreted by comparing the observed distances to those in graphite and other carbon structures. We highlight the main structural differences between atmospheric soot and graphite, and discuss the relevance of our findings to issues in atmospheric science.

2. Experimental

The measured soot particles are aggregates of many primary spherules and have diameters of ~250 nm. Measurements were carried out using a Philips CM20 transmission electron microscope (TEM), operating at 200 kV accelerating voltage. A standardised procedure was followed in order to obtain reproducible experimental results, including the following steps: (1) demagnetisation of all lenses, (2) setting a fix current for the objective lens, (3) positioning the thin sample to the focal plane of the objective lens (using Z-control), (4) setting fixed values for the condenser lenses (resulting both in a fixed convergence angle and a minimisation of the error of camera length due to interaction of the condenser and the objective lenses), and (5) focusing the diffraction pattern. Using this standardised procedure, deviations of the camera length proved to be $<0.3\%$, as determined in many tests (including the exchange of samples several times). The diffraction patterns were recorded on image plates, which give a linear response to the electron dose over six orders of magnitude. This large dynamic range is essential for quantifying the intensity distribution.

For obtaining atomic distances from SAED patterns, we used the following procedure (Takagi et al., 2001; Hirotsu et al., 2003; Lábár et al., 2003). Diffracted intensity was measured on the image plates within an adequate $Q = 4\pi \sin\theta/\lambda$ range (where θ and λ are the Bragg angle and the wavelength of the electron beam, respectively), up to a Q_{max} value where the experimentally observed undulations attenuated completely. Integrated diffracted intensities (I_{exp}) were retrieved using the Process Diffraction software (Lábár and Adamik, 2001). I_{exp} was then used for obtaining the reduced interference function ($Q \cdot i(Q)$), according to the following equation:

$$Q \cdot i(Q) = Q \cdot (I_{exp} - f^2)/f^2,$$

where f is the atomic scattering factor of carbon for electron radiation.

In the next step, the Fourier transform of $Q \cdot i(Q)$ was calculated, resulting in the reduced correlation function $G(r)$:

$$G(r) = 4\pi r \rho_0 [g(r) - 1],$$

where ρ_0 is the average density of the material, and $g(r)$ is the pair distribution function (PDF). Since $g(r) = \rho(r)/\rho_0$, where $\rho(r)$ is the density at r distance from the origin, the PDF is essentially a frequency distribution of individual atomic distances. The precision of the measurement depends on the applied Q range and decreases towards larger bond distances. The accuracy of the method was tested by measuring a 10-nm-thick, self-supporting nanocrystalline Al film. In the range of short (up to the third-nearest neighbour) and medium (up from the third-nearest neighbour) distances, accuracies of ± 0.001 and $\pm 0.002-0.003$ nm were measured, respectively.

For the present study, we selected two aerosol samples in which the individual particle types were previously characterised. One sample contains particles from the smoke of a savanna fire, and the other sample can be regarded as representative of a moderately polluted, rural aerosol in Central Europe. The samples were collected onto lacey Formvar + carbon-coated Cu TEM grids that were placed on the second and third stages of three-stage impactors with nominal cut-off diameters of 2 and 1 μm (in Africa and Europe, respectively). No further specimen treatment was applied after collection. Both samples contain carbonaceous particles abundantly, including soot, tar ball, and various organic particles. The savanna smoke sample was collected in Kruger National Park, South Africa (17 August 2000) during the Southern African Regional Science Initiative (SAFARI) 2000 experiment, from the young (several minutes old) smoke of a flaming fire. Aerosol particles in this sample were described in detail by Pósfai et al. (2003). The other sample was collected at a meteorological station (K-puszta) in Hungary, on 11 August 2004. Some of the typical particles from this site have been reported by Pósfai et al. (2004). The origin of soot particles in this continental sample is unknown. Distant traffic, industrial and household emissions could have contributed to the sample. However, at the time of the sampling a large number of agricultural fires were burning in the region (http://firemaps.geog.umd.edu), making biomass burning a likely source of soot in this sample as well.

Besides crystallographic data of graphite, samples of amorphous carbon and kerogen were used for comparison with the aerosol soot samples. Magnetron-sputtered amorphous carbon was produced on NaCl substrate in Ar atmosphere at room temperature, under a pressure $<10^{-7}$ mbar. The thickness of the amorphous carbon samples ranged between 0.5 and 40 nm. TEM samples were prepared by floating the carbon films off the substrate in distilled water and by placing them on Cu grids.

In order to test the effect of hydrogen content on the electron scattering, we measured a kerogen sample with a H/C ratio of 0.61. The kerogen sample was prepared and its composition analysed as described by Brukner-Wein et al. (2000). TEM samples of kerogen were prepared by grinding the kerogen powder under liquid nitrogen to avoid artefacts resulting from its plasticity (Oberlin et al., 1980), and a drop of the suspension with distilled water was placed onto the lacey carbon Cu grid. Measurements were made near liquid nitrogen temperature (−175 °C), in order to avoid structural changes resulting from electron beam heating. For the diffraction measurements, those parts of the sample were selected which covered the holes of the carbon-coated Formvar film. In this way, scattering contribution from the carbon coating was excluded from the measurements.

The compositions of soot particles and the kerogen sample were measured by energy-dispersive X-ray spectrometry (EDS), using a NORAN EDS detector attached to the electron microscope that can detect signals from elements heavier than boron. The soot particles contained >95 at% C, ~1–3 at% O and <1 at% Si and K. The kerogen

sample contained 95 at% C, 3–4 at% O and <1 at% S, Fe and Cl, the Cl probably present as a result of the acidic separation that was applied in sample preparation.

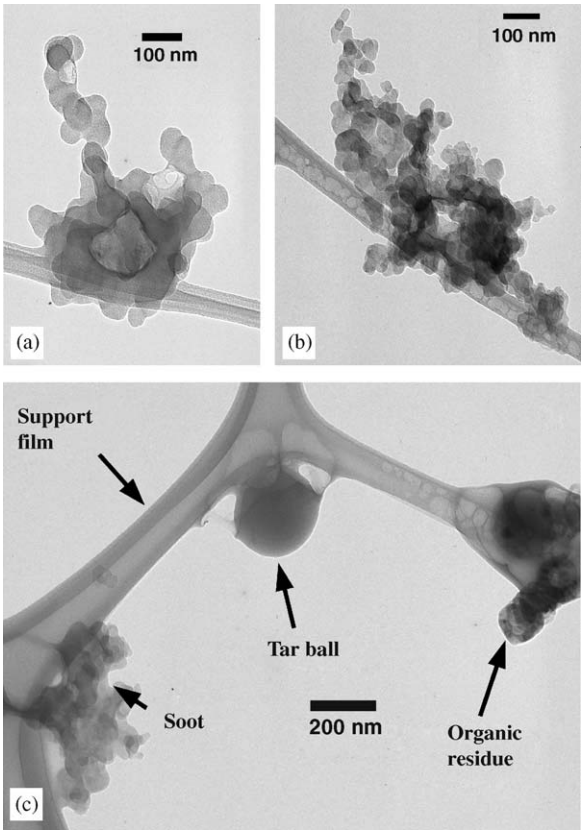

Fig. 1. TEM bright-field images of typical carbonaceous particles from atmospheric aerosol samples. (a) Soot particle from the smoke of a savanna fire in Kruger National Park, South Africa. (b) Soot particle from the Central European troposphere (K-puszta, Hungary). (c) Other types of carbonaceous particles from the Central European troposphere (K-puszta, Hungary).

3. Results

TEM bright-field images and SAED patterns of some of the distinct types of carbonaceous particles are presented in Figs. 1 and 2, respectively. The diameters of individual nanospheres within soot particles are typically ~50 nm in the savanna smoke sample (Fig. 1a), whereas in the continental sample nanospheres having diameters of 20–30 nm also occur (Fig. 1b). The SAED pattern obtained from the soot particle shown in Fig. 1a exhibits three distinct rings, corresponding to the real-space d values that are indicated in Fig. 2a. These distances are close to the d(00.2), d(10.1) and d(11.2) values of $P6_3/mmc$ graphite, respectively (Wyckoff, 1963). Consistent with representative HRTEM images of soot (Pósfai et al., 1999; Li et al., 2003; Wentzel et al., 2003), the first diffraction ring corresponds to the distance between adjacent curved graphene layers. This "basal distance" is larger by 8–10% than the d(00.2) value of graphite. The larger interlayer distance is not unique for soot, but a common feature of curved carbon nanostructures (Jäger et al., 1999). In addition to soot, we performed preliminary measurements on two other types of carbonaceous particles. We wished to test whether the different amorphous particle types produce distinct features in SAED patterns. Tar balls (Fig. 1c) are typically 100–200-nm large, amorphous spherules (Pósfai et al., 2004; Hand et al., 2005). Their diffraction patterns differ from that of soot: intensity maxima appear around 2.0 and 1.1 Å, whereas the 3.5 Å ring is absent (Fig. 2b). Organic compounds occur in the K-puszta sample in various particle types, including internally mixed ammonium sulphate/organic particles. After the sulphate component of such particles is sublimated with the electron beam, an organic residue remains.

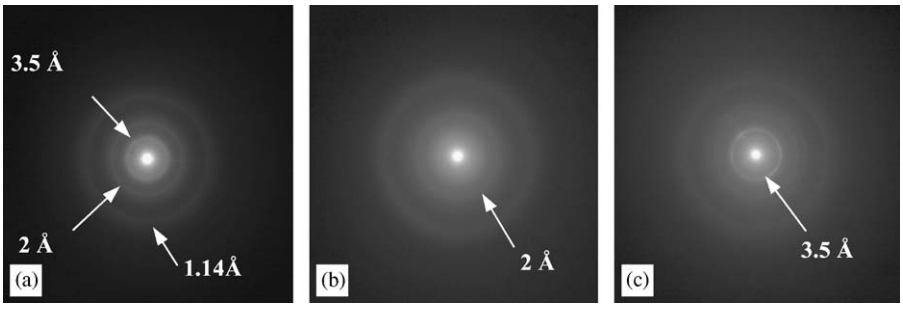

Fig. 2. Selected-area electron diffraction patterns of (a) the soot particle in Fig. 1a, (b) the tar ball in Fig. 1c and (c) the residue of the ammonium sulphate/organic particle in Fig. 1c.

Such a residue is shown in Fig. 1c, and its SAED pattern is presented in Fig. 2c. Faint, diffuse rings in the SAED pattern suggest a microstructure distinct from those of both soot and tar ball particles.

The focus of the present study is soot nanostructure. Altogether 11 soot particles were measured in the two samples. PDFs derived from three selected SAED patterns are presented in Fig. 3a. Maxima of the PDF represent frequently occurring atomic distances. However, atomic distances very close to one another cannot be resolved due to peak broadening. Generally, peak width is affected by both the Q-range of the measurement and the ordering state of the material. Since we applied a large enough Q-range that included all measurable diffracted intensity, information loss in the reciprocal space is unlikely to contribute to the peak broadening. Thus, the broad peaks in the PDFs are the consequence of the disordered structure of soot.

Despite the apparent disorder in soot particles, the first two prominent peaks in the PDFs appear at values that can be interpreted as the first- and second-neighbour intralayer atomic distances (L1 and L2) of layered (sp^2) carbon structures, respectively. The third peak in the PDFs likely corresponds to the first interlayer atomic distance, B1 (L and B denote distances between intra- and interlayer carbon atoms, respectively, and the numbers refer to the rank of neighbours).

Interatomic distances obtained from the first three peaks are plotted in Fig. 4 together with similar distances measured in amorphous carbon and kerogen. The interatomic distances for graphite (Wyckoff, 1963) are also shown. Even though the measured interatomic distances in the different samples are close to each other, ranges of values can be identified that are characteristic of the different forms of carbon. The values for amorphous carbon show the narrowest range; a larger scatter in the data points measured for soot and kerogen may reflect real structural deviations.

The first-neighbour intralayer C–C distance (L1) in soot varies between 0.133 and 0.137 nm (Fig. 4a), and is significantly shorter than the corresponding values in crystalline carbon polymorphs and amorphous carbon (Fig. 3b). As discussed above, the PDF curves can be regarded as histograms of atomic distances. Since the peaks are relatively broad, the first peak in Fig. 3 may include the atomic distances between 0.11 and 0.142 nm, typical of the C–H distance, and the first-neighbour intralayer C–C distance in a graphene sheet,

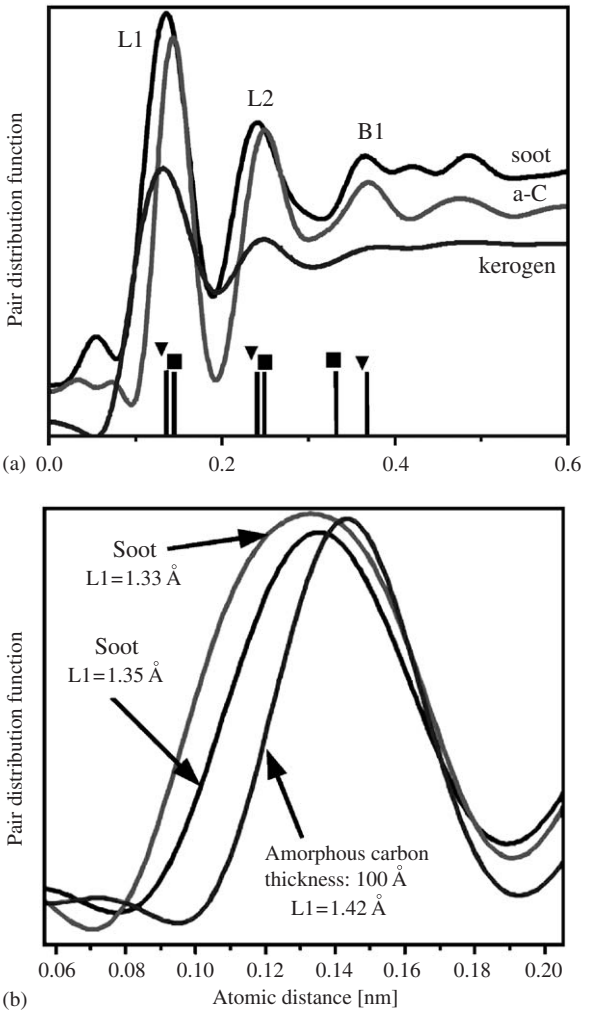

Fig. 3. (a) Pair distribution functions derived from measurements on a soot particle and on two reference materials (amorphous carbon (marked "a-C") and kerogen); ▼: measured atomic distance in soot; ■: atomic distance in graphite (Wyckoff, 1963). L1 and L2 denote peaks that correspond to the first- and second-neighbour intralayer C–C distances, respectively, and B1 denotes the peak that corresponds to the shortest interlayer C–C distance. (b) A close-up of the first (L1) peaks of two soot particles and of amorphous carbon.

respectively. The observed maxima between 0.133 and 0.137 nm in soot suggest a distinct shift of the most frequent atomic distance towards lower values with respect to graphite and amorphous carbon.

The second-neighbour intralayer atomic distance (L2) varies between 0.236 and 0.246 nm in soot (Fig. 4b). These values are slightly shorter than the corresponding distance in graphite (0.246 nm) and in amorphous carbon. The third-neighbour intralayer atomic distance of graphite (0.284 nm), which

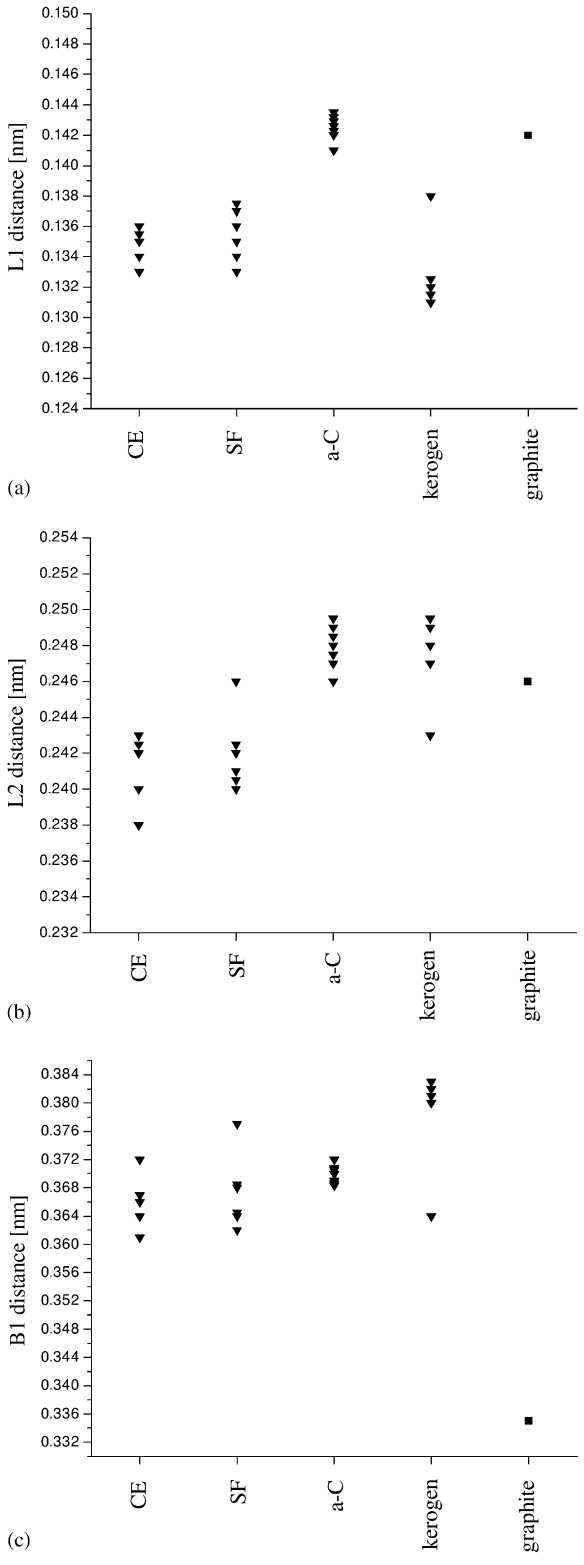

corresponds to the longest diagonal of the carbon hexagons, cannot be resolved or is absent in the PDFs of soot. In some cases a small peak appears at around 0.284 nm. However, small peaks in the PDF may be present due to the artificial cut-off in the reciprocal space during data processing. Alternatively, a small broad peak in the PDF that represents a real interatomic distance, may cause an elevated minimum value instead of a distinct peak, making this interatomic distance undetectable.

The next prominent peak in the PDFs of soot (Fig. 3a) appears between 0.361 and 0.377 nm. Although some overlap with the fourth C–C distance within the graphene-like sheet (0.375 nm in graphite) cannot be excluded, we interpret this atomic distance as mainly representative of the first interlayer atomic distance (B1). In graphite, the two shortest distances between carbon atoms in adjacent layers are 0.335 and 0.363 nm. In soot, this distance is shifted towards larger values, which is in agreement with the HRTEM observations. A shift of similar magnitude can be observed in amorphous carbon as well. The B1 values for kerogen must be considered with care because of enhanced peak broadening (Fig. 3a); nevertheless, they appear to be larger than those of graphite. Satisfactory explanation for the larger B1 distance in soot is still lacking; presumably, it is related to the random orientations of the graphene-like fragments.

4. Discussion

Interatomic distances derived from SAED patterns provide information on the possible bond types. The goal of the present study is to identify possible bond types and structural elements within

Fig. 4. Atomic distances in atmospheric soot as measured using selected-area electron diffraction. For comparison, the corresponding atomic distances in magnetron-sputtered amorphous carbon (7 measurements of 7 samples, with the thickness ranging from 0.5 to 40 nm) and in kerogen with a H/C ratio of 0.61 (5 measurements) are also shown. Atomic distances of graphite were calculated based on structural data of Wyckoff (1963). CE: Central European sample; SF: savanna smoke sample from the SAFARI 2000 experiment; a-C: amorphous carbon. (a) L1 distance, (b) L2 distance (c) B1 distance. Note that one of the five measurements performed on kerogen resulted in interatomic distances of 0.138 (a), 0.243 (b) and 0.364 nm (c) (outlying points in the diagrams) and a larger correlation length than in the case of the other particles (not shown), suggesting a structure that is distinctly different from the structure indicated by the other four measurements.

the graphene-like layers of soot. The atomic distances were found to be essentially the same in all of the 11 soot particles that were measured in the two samples. The first-neighbour (L1) distances in soot are shorter (0.133–0.137 nm) than the corresponding distances in graphite. This indicates the presence of a significant amount of small-sized aromatic moieties in the graphene-like sheets as is detailed below.

Interatomic distances of various carbon structures are listed in Table 1. The first-neighbour distance, i.e., the C–C bond length varies between that of the single bond in diamond, an sp^3 hybridisation state of carbon (0.154 nm), and of the C–C double bond, such as in ethylene (0.133 nm). For instance, in graphite, the sp^2 crystalline polymorph, the C–C bond length is 0.142 nm.

The simplest aromatic compound, benzene, has six C–C bonds of equal length (0.139 nm), which are slightly shorter than the intralayer atomic distance (L1) in graphite. The asymmetric electronic structure of polycyclic aromatic molecules leads to C–C bonds, which are either shorter or longer than in benzene. Bond lengths between two carbon atoms that are both surrounded by three other carbon atoms varies between 0.140 and 0.143 nm in naphtalene (2 rings), pyrene (4 rings) and coronene (7 rings) (Table 1). These carbon atoms are in the interior of the molecule, and their atomic environment is identical to that of carbon atoms in a graphene sheet, and their bond lengths deviate only by 0.001–0.002 nm from the bond length in graphite. Some of the C–C bond lengths between carbon atoms on the perimeter of the aromatic molecule, i.e., between carbon atoms that both have one hydrogen and two carbon neighbours, are significantly shorter (by 0.006–0.008 nm) than in the interior of the molecule and in graphite. The length of this bond type varies from 0.134–0.136 nm in pyrene and coronene (Table 1). Whereas the average value of the C–C bond lengths in polycyclic aromatic molecules containing up to 7 rings is very close to the C–C bond length of benzene, in larger aromatic molecules it approaches the L1 value of graphite.

Electron scattering is also sensitive to the presence of C–H bonds, which are abundant in small-sized polycyclic aromatic compounds. These C–H bonds have a typical bond length of 0.108–0.112 nm (Weast, 1972). The scattering power of hydrogen is relatively weak; it varies between 20% and 25% of that of carbon, in function of Q (Ibers, 1958). Therefore, the contribution of C–H atomic distances to the total PDF must be smaller than that of the C–C bonds. However, the measured very short L1 values suggest that the effect of C–H atomic distances cannot be neglected, and the L1 peak in the PDF curve results from the combined contributions of first-neighbour C–C and C–H distances.

In order to test the contribution from C–H atomic pairs to the total electron scattering, we

Table 1
Bond lengths and atomic distances in crystalline carbon polymorphs, carbon molecules and aromatic hydrocarbons

	C–C	C–C2	C–C3
C–C atomic distances in crystalline polymorphs [nm]			
Diamond	0.154	0.252	0.295
Graphite	0.142	0.246	0.284
C–C atomic distances in carbon molecules [nm]			
C60 pentagon	0.146	0.237	
C60 hexagon	0.139; 0.146	0.247	0.285
C70 pentagon	0.140	0.226	
C70 hexagon	0.140–0.142	0.242–0.244	0.277–0.282
Atomic distances in hydrocarbon molecules [nm]			
Benzene (C_6H_6)	0.140	0.241	0.278
Naphtalene ($C_{10}H_8$)	0.136–0.142	0.241–0.245	0.280–0.282
Pyrene ($C_{16}H_{10}$)	0.134–0.143		
Coronene ($C_{24}H_{12}$)	0.136–0.143		
Fluorene pentagon	0.143–0.150		
Fluorene hexagon	0.138–0.143		
C═C double bond length: 0.133 nm			

measured a kerogen sample with a H/C ratio of 0.61. Although this H/C ratio is significantly larger than the value determined by thermal methods for soot (0.15) (Huffman, 1996), measurements on this kerogen sample allow us to analyse the effects of H–C bonds on the PDF curves.

Four measurements resulted in very similar PDFs, with L1 distances as short as 0.131 nm (Fig. 4a), suggesting that the first peak in the PDF can result from a superposition of the first-neighbour C–C and C–H distances. A high degree of disorder results in a single peak, without any clearly visible splitting or a discernible shoulder. The results imply a higher H/C ratio in the measured kerogen than in soot, which has L1 distances from 0.133 to 0.137 nm.

In magnetron-sputtered amorphous carbon, we measured first-neighbour C–C distances that coincide with the first intralayer atomic distance (L1) of graphite (0.142 ± 0.001 nm) (Fig. 4a). The amorphous carbon sample was produced in an Ar atmosphere and may also contain buckled graphene fragments and thus five-membered rings; however, it is free of hydrogen. Thus, pyrene- or coronene-like aromatic structures, containing both short C–C (0.134–0.136 nm) and C–H bonds cannot form in it, resulting in longer first-neighbour C–C distances than in soot.

Some sp^2 carbon structures also contain five-membered rings besides the six-membered rings. In the surroundings of the five-membered rings, similarly to the case of the carbon molecules, shorter first-neighbour C–C distances are present than in graphite (Table 1). However, the five-membered rings cause a reduction of the C–C distance by only 0.002–0.003 nm with respect to the L1 value of graphite, and so are unlikely to be responsible for the shorter distances measured in soot.

The observations on amorphous carbon and kerogen support our interpretation that the measured low values (0.133–0.137 nm) of the first intralayer atomic distance (L1) in soot can be explained by overlapping peaks in the PDF, which represent the C–C and C–H atomic distances. These peaks cannot be resolved because of the peak broadening that is caused by the disordered structure. The superposition of first-neighbour intralayer C–C distances of 0.134–0.143 nm (Table 1) and C–H distances of 0.108–0.112 nm of small-sized aromatic clusters results in a single broad peak in the PDF of soot. If some C–C double bonds are also present within the soot nanospherules, they are not expected to cause a splitting of the peak.

The hydrogen content of amorphous carbon affects the low-loss part of the EEL spectrum as well. The incorporation of up to 30% hydrogen reduces the plasmon energy of amorphous carbon by ~2 eV from its typical value of 24 eV (Chen et al., 2005, Calliari et al., 2006). In order to determine the hydrogen content of atmospheric soot, we performed EEL measurements on the SF soot sample. The plasmon peak was found to be present at ~22.2 eV, which is consistent with literature data for hydrogen-bearing amorphous carbon and suggests the presence of hydrogen in the measured atmospheric soot.

Aromatic structures of tarry species and soot formed in an ethylene/oxygen flame were studied using UV–visible spectroscopy (Apicella et al., 2004). The optical properties of young soot were found to be similar to those of asphaltanes. Asphaltanes are considered to consist of aromatic systems composed of 4–10 rings, joined by aliphatic bridges (Groenzim and Mullis, 2000). The similarity between the optical properties of young soot and asphaltenes suggest similar medium-range structures that are dominated by small-sized aromatic systems. An analysis of the fine structure of the carbon peak in EEL spectra of atmospheric soot also suggests a mixture of bond types that are characteristic of graphite and of hydrocarbons (Katrinak et al., 1992).

Polycyclic aromatic molecules are flat molecules; disregarding peripheral hydrogen atoms, they resemble fragments of a graphene layer. In contrast, if a five-membered ring is inserted among the hexagons, a slight curvature forms (as in the structure of corannulene, $C_{20}H_{10}$) (Hanson and Nordman, 1976). As the number of five-membered rings increases, the curved geometry is enhanced. The second-neighbour C–C distances (L2 values) measured in atmospheric soot may imply the presence of five-membered rings that lead to the buckling of the aromatic clusters. This interpretation is in agreement with HRTEM observations that show a concentrical, onion-like structure of individual soot nanospherules in a wide variety of soot samples, including diesel engine soot (Su et al., 2004), atmospheric soot (Pósfai et al., 1999; Li et al., 2003; Wentzel et al., 2003) and soot produced by the thermal pyrolysis of hydrocarbons (Vander Wal and Tomasek, 2004). Nevertheless, we cannot exclude that the presence of C–H bonds and the related

deviation of the hexagonal rings from the ideal geometry also contribute to the reduction of the L2 distance.

The sizes of aromatic moieties affect the optical properties of soot. The growth of the size of the aromatic system from benzene to molecules containing a larger number of rings leads to an increase of the absorption wavelength. That is, the larger the molecule, the lower the energy that is needed for the electronic transition (Clar, 1974). At a particular wavelength, the absorption coefficients of small-sized aromatic compounds are generally smaller than that of mature soot, indicating an increase in the degree of polymerisation as soot matures (Apicella et al., 2004). It follows that the young or mature character of aerosol soot, which can be inferred from the dominant size of the aromatic structures, has noticeable influence on the absorption properties. We note that in combustion science studies, the terms 'young' and 'mature' refer to soot particles formed in different parts of the flame; thus, according to this terminology, all soot particles are 'mature' in atmospheric samples. Nevertheless, soot maturation likely continues in the atmosphere.

Since we studied soot particles in two samples only, at present we do not know whether the measured short first-neighbour distances are characteristic for most atmospheric soot particles, or they are typical for relatively young soot only. At the same time, it has to be considered that the probable source of both samples is biomass burning. This may explain that similar values were found as the most frequent atomic distances in all of the 11 measured particles, independent of the sample.

5. Conclusions

SAED measurements were used to determine interatomic distances in soot particles from two atmospheric samples. Based on comparisons with interatomic distances in amorphous carbon and in a kerogen sample with a high H/C ratio, we propose that hydrocarbons are present in atmospheric soot particles in the form of small-sized aromatic moieties. The first peak in the PDF presumably arises from a superposition of the C–C and C–H distances in the aromatic clusters. This predominant atomic distance is smaller than the corresponding value in graphite and suggests the presence of hydrocarbons containing a small number of rings, and having a high molar ratio of hydrogen. This finding has implications for the optical properties of soot, since the absorption coefficient depends on the size of aromatic moieties within the graphene-like sheets.

Quantitative electron diffraction proved to be an independent and efficient alternative to the commonly used spectroscopic methods for studying the structure of atmospheric soot particles. The absorption properties of individual, morphologically well-defined carbonaceous particles can be assessed through an analysis of their aromatic characters. Although the present study focuses on soot, our preliminary experiments suggest that atomic distances in other, morphologically distinct carbonaceous particles (such as tar balls and other organic particles) can also be derived from SAED patterns. In the future, we plan to apply the quantitative SAED technique to systematic studies of different types of soot and other carbonaceous atmospheric aerosol particles.

Acknowledgements

We thank Csanád Sajgó for providing the kerogen sample. We are grateful for the critical and helpful comments of two anonymous referees. This work was supported by the Hungarian Science Fund (OTKA T043437 to JL, OTKA PF63973 to VKK and OTKA-Ts040903 to MP).

References

Abrahamson, J., 1977. Saturated platelets are new intermediates in hydrocarbon pyrolysis and carbon formation. Nature 266, 323–327.

Andreae, M.O., 2001. The dark side of aerosols. Nature 409, 671–672.

Apicella, B., Alf, M., Barbella, R., Tregrossi, A., Ciajolo, A., 2004. Aromatic structures of carbonaceous materials and soot inferred by spectroscopic analysis. Carbon 42, 1583–1589.

Bockhorn, H. (Ed.), 1994. Soot Formation in Combustion: Mechanisms and Models. Springer, Berlin.

Bond, T.C., Bussemer, M., Wehner, B., Keller, S., Charlson, R.J., Heintzenberg, J., 1999. Light absorption by primary particle emissions from a lignite burning plant. Environmental Science and Technology 33, 3887–3891.

Brukner-Wein, A., Sajgó, Cs., Hetényi, M., 2000. Comparison of Pliocene organic-rich lacustrine sediments in twin craters. Organic Geochemistry 31, 453–461.

Calliari, L., Filippi, M., Laidani, N., Anderle, M., 2006. The electronic structure of carbon films deposited in rf argon–hydrogen plasma. Journal of Electron Spectroscopy and Related Phenomena 150, 40–46.

Chen, G.Y., Stolojan, V., Silva, S.R.P., Herman, H., Haq, S., 2005. Carbon spheres generated in dusty plasmas. Carbon 43, 704–708.

Clar, E., 1974. Polycyclic Aromatic Hydrocarbons. Academic Press, London, New York.

Gelencsér, A., 2004. Carbonaceous Aerosol. Springer, Berlin, 350pp.

Goel, A., Hebgen, P., Vander Sande, J.B., Howard, J.B., 2002. Combustion synthesis of fullerenes and fullerenic nanostructures. Carbon 40, 177–182.

Groenzim, H., Mullis, O.C., 2000. Molecular size and structure of asphaltanes from various sources. Energy & Fuel 14, 677–684.

Hand, J.L., Malm, W.C., Laskin, A., Day, D., Lee, T., Wang, C., Carrico, C., Carrillo Jr., J., Cowin, J.P., Collett, J., Iedema, M.J., 2005. Optical, physical, and chemical properties of tar balls observed during the Yosemite Aerosol Characterization Study. Journal of Geophysical Research 110, D21210.

Hanson, J.C., Nordman, C.E., 1976. The crystal and molecular structure of corannulene, $C_{20}H_{10}$. Acta Crystallographica B 32, 1147–1153.

Hirotsu, Y., Ohkubo, T., Bae, I.T., Ishimaru, M., 2003. Electron diffraction structure analysis for amorphous materials. Materials Chemistry and Physics 81, 360–363.

Huffman, H.D., 1996. The reconstruction of aerosol light absorption by particle measurements at remote sites: an independent analysis of data from the IMPROVE network—II. Atmospheric Environment 30, 85–99.

Ibers, J.A., 1958. Atomic scattering amplitudes for electrons. Acta Crystallographica 11, 178–183.

Jacobson, M.Z., 2001. Strong radiative heating due to the mixing state of black carbon in atmospheric aerosols. Nature 409, 695–697.

Jäger, C., Henning, Th., Schlögl, R., Spillecke, O., 1999. Spectral properties of carbon black. Journal of Non-Crystalline Solids 258, 161–179.

Katrinak, K.A., Rez, P., Buseck, P.R., 1992. Structural variations in individual carbonaceous particles from an urban aerosol. Environmental Science and Technology 26, 1967–1976.

Lábár, J.L., Adamik, M., 2001. ProcessDiffraction V1.2: new possibilities in manipulating electron diffraction ring patterns. Microscopy and Microanalysis 7, 372–373.

Lábár, J.L., Kovács, A., Barna, B.P., Hanada, T., Ishimaru, M., Hirotsu, Y., Bae, I.T., 2003. Correlation between short range order and composition in an amorphous Al–Pt alloy, existing in a wide compositional range. Abstracts of EMAS'2003 (Eighth European Workshop on Modern Developments and Applications in Microbeam Analysis), 310pp.

Lahaye, J., 1992. Particulate carbon from the gas phase. Carbon 30, 309–314.

Li, J., Pósfai, M., Hobbs, P.V., Buseck, P.R., 2003. Individual aerosol particles from biomass burning in Southern Africa: 2. Compositions and aging of inorganic particles. Journal of Geophysical Research 108, 8484.

Mertes, S., Dippel, B., Schwarzenböck, A., 2004. Quantification of graphitic carbon in atmospheric aerosol particles by Raman spectroscopy and first application for the determination of mass absorption efficiencies. Journal of Aerosol Science 35, 347–361.

Oberlin, A., Boulmier, J.L., Villey, M., 1980. Electron microscopic study of kerogen microtexture. In: Durend, B. (Ed.), Selected Criteria for Determining the Evolution Path and Evolution Stage of Kerogen. Éditions Technip, Paris, pp. 191–241.

Penner, J.E., Zhang, S.Y., Chuang, C.C., 2003. Soot and smoke aerosol may not warm climate. Journal of Geophysical Research 108, 4657.

Pósfai, M., Anderson, J.R., Buseck, P.R., 1999. Soot and sulfate aerosol particles in the remote marine troposphere. Journal of Geophysical Research 104, 21685–21693.

Pósfai, M., Simonics, R., Li, J., Hobbs, P.V., Buseck, P.R., 2003. Individual aerosol particles from biomass burning in southern Africa: 1. Compositions and size distributions of carbonaceous particles. Journal of Geophysical Research 108, 8483.

Pósfai, M., Gelencsér, A., Simonics, R., Arató, K., Li, J., Hobbs, P.V., Buseck, P.R., 2004. Atmospheric tar balls: particles from biomass and biofuel burning. Journal of Geophysical Research 109, D06213.

Schmid, H., Laskus, L., Abraham, H.J., Baltensperger, U., Lavanchy, V., Bizjak, M., Burba, P., Cachier, H., Crow, D., Chow, J., Gnauk, T., Even, A., ten Brink, H.M., Giesen, K.-P., Hitzenberger, R., Hueglin, C., Maenhaut, W., Pio, C., Carvalho, A., Putaud, J.-P., Toom-Sauntry, D., Puxbaum, H., 2001. Results of the "carbon conference" international aerosol carbon round robin test stage I. Atmospheric Environment 35, 2111–2121.

Su, D.S., Jentoft, R.E., Müller, J.-O., Rothe, D., Jacob, E., Simpson, C.D., Tomovi, Ž., Müllen, K., Messerer, A., Pöschl, U., Niessner, R., Schlögl, R., 2004. Microstructure and oxidation behaviour of Euro IV diesel engine soot: a comparative study with synthetic model soot substances. Catalysis Today 90, 127–132.

Takagi, T., Ohkubo, T., Hirotsu, Y., Murty, B.S., Hono, K., Shindo, D., 2001. Local structure of amorphous $Zr_{70}Pd_{30}$ alloy studied by electron diffraction. Applied Physics Letters 79, 485–487.

Vander Wal, R.L., Tomasek, A.J., 2004. Soot nanostructure: dependence upon synthesis conditions. Combustion and Flame 136, 129–140.

Weast, R.C. (Ed.), 1972. Handbook of Chemistry and Physics. The Chemical Rubber Co. p. F-173.

Wentzel, M., Gorzawski, H., Naumann, K.-H., Saatho, H., Weinbruch, S., 2003. Transmission electron microscopical and aerosol dynamical characterization of soot aerosols. Journal of Aerosol Science 34, 1347–1370.

Wyckoff, R.W.G., 1963. Crystal Structures. Interscience Publishers, New York.